NJC

Accepted Manuscript

This article can be cited before page numbers have been issued, to do this please use: R. Ganduri, V. Singh, A. Biswas, K. D. Prasad, K. Sekar, K. N. Balaji and G. R. N. Tayur, *New J. Chem.*, 2018, DOI: 10.1039/C8NJ00852C.

ROYAL SOCIETY OF CHEMISTRY

rsc.li/njc

View Article Online
DOI: 10.1039/C8NJ00852C

Structural and biological evaluation of halogen derivatives of 1,9-pyrazoloanthrones towards the design of specific potent inhibitor of c-Jun-N-terminal kinase (JNK)

Ramesh Ganduri,[a] Vikas Singh,[b] Ansuman Biswas,[c] Karothu Durga Prasad,[a] Kanagaraj Sekar,[d] Kithiganahalli N. Balaji[b] and Tayur N. Guru Row*[a]

[a] *Solid State and Structural Chemistry Unit, Indian Institute of Science, Bangalore 560012, Karnataka, India*
E-mail: gururow@iisc.ac.in; Fax:+91-80-23601310; Tel: +91-80-22932796
[b]*Department of Microbiology and Cell Biology, Indian Institute of Science, Bangalore 560012, Karnataka, India*
[c] *Department of Physics, Indian Institute of Science, Bangalore 560012, Karnataka, India*
[d] *Department of Computational and Data Sciences, Indian Institute of Science, Bangalore 560012, Karnataka, India*

Abstract

c-Jun N-terminal kinase (JNK), a member of MAPK family, is associated with a variety of diseases and immune responses. To dissect the mechanistic role of JNKs in such processes, specific inhibitor for JNKs holds great value. SP600125 is widely used inhibitor of JNKs despite its non-specific activity. In an effort to obtain better specific inhibitors, three anthrapyrazolone halogenated derivatives have been synthesized and characterized. Among the three derivatives, 5-chloro-2-(2-chloroethyl) dibenzo[*cd,g*] indazol-6(2*H*)-one is clearly established as a specific inhibitor of JNK with augmented expression of chemokines in LPS-activated macrophages based on modelling studies followed by *in vitro* and *ex vivo* evaluation.

View Article Online
DOI: 10.1039/C8NJ00852C

1. Introduction

JNKs are serine/threonine protein kinases which belong to the mitogen-activated protein kinases (MAPKs) family. Notably, there are three distinct genes that codes for JNK1, JNK2 and JNK3 which results in expression 10 isoforms of JNKs via alternative splicing. JNKs play a central role in host inflammatory responses and they have been implicated in a wide range of inflammation associated disorders such as arthritis and atherosclerosis.[1–3] The host immune responses to Gram-negative bacteria cell wall-derived LPS is characterized by the recruitment of immune cells such as macrophages and neutrophils at the site of infection. Moreover, infiltrated immune cells induce inflammation which is mediated by localized production of chemokines.[4,5] Chemokines are the class of highly specialized cytokines that are implicated in a wide range of biological processes including cellular stress, cancer, angiogenesis and bacterial or viral pathogenesis.[6–8] Growing body of evidences indicates a significant contribution of c-Jun N-terminal kinase (JNK) in the regulation of chemokines expression.[9–11] JNK-induced phosphorylation of c-Jun at ser63 or ser73 facilitates its interaction with c-Fos which in turn form a complex with transcription factor activator protein 1 (AP-1) and regulate host immune responses.[12–14] In light of current literature it becomes important to design and synthesize potent and JNK-specific inhibitors with minimal or no off-target effects to attain deeper understanding in JNK mediated signalling mechanism and immune responses. Among existing JNKs inhibitors,[15] SP600125 (anthra [1, 9] pyrazol-6 (2*H*)-one or 1,9-pyrazoloanthrone),[16] inhibits JNK1/2/3 with specificity and subsequently inhibits activation of c-Jun. Although SP600125 is utilized as a selective JNKs inhibitor, its off-target effect on other kinases such as PI3K (p110δ), p70 ribosomal protein kinase (S6K1) and mps1 invited new disputes in its utility as a selective inhibitor for JNKs.[17–21] In an effort to develop improved inhibitors with reduced or completely blocked off target effects, we have shown that N-alkyl substituted pyrazoloanthrone derivatives regulate inhibiting

View Article Online
DOI: 10.1039/C8NJ00852C

potential and JNKs activity with minimal off-target effect on other mitogen activated protein kinases unlike the commercially available 1,9-pyrazoloanthrone (SP600125).[22] Several N-alkyl and hydroxyl substituted derivatives of 1,9-pyrazoloanthrone derivatives have been designed, synthesised and tested *in vitro* for analysis of JNK inhibition at varied concentrations. The results revealed that among all analogues of 1,9-pyrazoloanthrone (SP600125), propyl, butyl and hydroxyl substituted pyrazoloanthrone scaffolds confer better binding energies along with notable inhibitory effect on JNKs activity.[23] Such detailed biochemical evaluation of selective JNK inhibition allows for the identification of specific drugs to treat diseases like sepsis on one hand and on the other, provide complete characterization of biological functions of JNK.[23]

Intermolecular interactions like hydrogen bonds, hydrophobic contacts and van der Waals forces play a decisive role in both structural and functional aspects in chemical biology. In recent years, halogen bonds (XB) which are demonstrated to be highly directional among non-covalent interactions have been identified to provide well directed adhesive contacts for protein-ligand interactions[24,25] and are increasingly being explored based on structural and theoretical estimates of energies.[26,27] Experimental and theoretical charge density analysis establish the highly directional and attractive nature of halogen bonded interactions in terms of the so called σ-hole concept.[28–31] Moreover, halogen derivatives are preferred as enzyme inhibitors since they improve the protein-ligand binding affinity, specificity along with tuning ADME/T properties.[32,33] Halogen bonds also provide sufficient binding energies to hold the molecule/s in the binding pocket resulting in heightened activity of the inhibitor. An examination of the Protein Data Bank (PDB) database[34] reveals sufficiently large number of structures with halogenated ligands suggesting the importance of halogen bonding for rational design of selective and potent inhibitors against the therapeutic targets.[35,36] The

View Article Online
DOI: 10.1039/C8NJ00852C

geometrical factors of halogen bonding for stabilizing inter- and intra-molecular interactions in biomolecules that can influence the ligand binding with protein have also been analyzed.[37]

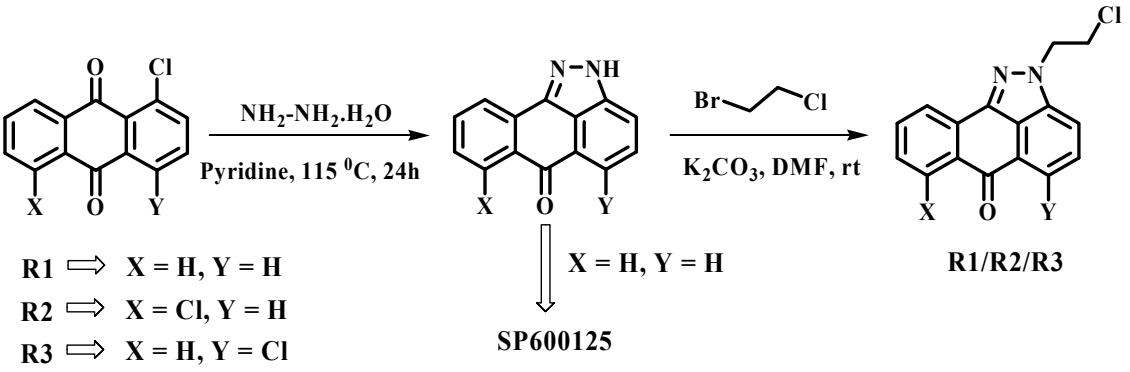

Scheme 1 Synthetic scheme for the three anthrapyrazolone halogen derivatives.

In the present study, three chloro derivatives of SP600125, 2-(2-chloroethyl) dibenzo[*cd,g*]indazol-6(2*H*)-one, 7-chloro-2-(2-chloroethyl)dibenzo[*cd,g*]indazol-6(2*H*)-one and 5-chloro-2-(2-chloroethyl)dibenzo[*cd,g*]indazol-6(2*H*)-one, (**R1, R2** and **R3 respectively;** Scheme 1) are examined based on the fact that halogen interactions provide highly directional and enhanced specificity towards JNK inhibitory binding.[23,24] Even though all three compounds depict halogen interactions in the binding pocket based on molecular dynamics simulations, compounds **R2** and **R3** imply stable halogen interactions at optimal distance for halogen bonding. Diffraction quality crystals could be grown only for **R2** and its crystal structure is reported. Indeed both **R2** and **R3** exhibit specific inhibition of JNK activity at lower concentrations with no off-target effects based on *in vitro* biological studies. However, compound **R3** depicts highly specific inhibition with minimal off target effects at significantly lower concentrations (<5 μM).[38]

View Article Online
DOI: 10.1039/C8NJ00852C

2. Results and Discussion

2.1. Synthesis

The compounds 2-(2-chloroethyl) dibenzo[*cd,g*]indazol-6(2*H*)-one, 7-chloro-2-(2 chloro ethyl)dibenzo[*cd,g*]indazol-6(2*H*)-one and 5-chloro-2-(2-chloroethyl) dibenzo[*cd,g*]indazol-6(2*H*)-one, **R1**, **R2**, and **R3** respectively (Scheme 1) have been synthesized. All three compounds were characterized by HR-MS and purity was assessed by the ^{1}H and ^{13}C-NMR spectroscopic techniques (Fig. S1a-S1i, ESI†).

2.2. Crystal Structure Description

Attempts to crystallize all three compounds resulted in diffraction quality crystals for only **R2**. Single crystals of 7-chloro-2-(2-chloroethyl)dibenzo[*cd,g*]indazol-6(2*H*)-one (**R2**), were grown from solvent mixture of Methanol/Tetrahydrofuran (70/30%, v/v) by slow solvent evaporation at ambient temperature. X-ray diffraction data were collected at 100K, structure was solved and refined in a monoclinic space group $P2_1/n$ with Z = 4 (Table 1). ORTEP with thermal ellipsoids and crystal packing of **R2** are shown in Fig. 1**.** It is of interest to note that there are intermolecular interactions involving both chlorine atoms, Cl1 and Cl2 (two C-H...Cl contacts; 2.913Å and 2.838Å and one Cl1...Cl2 halogen bond; 3.251Å; angles ∠C–Cl1···Cl2 = 151.84°; ∠C–Cl2···Cl1 = 163.59° respectively suggesting a Type-I geometry),[30] which point out to the possibility of generating halogen atom involved interactions in the binding pocket.

View Article Online
DOI: 10.1039/C8NJ00852C

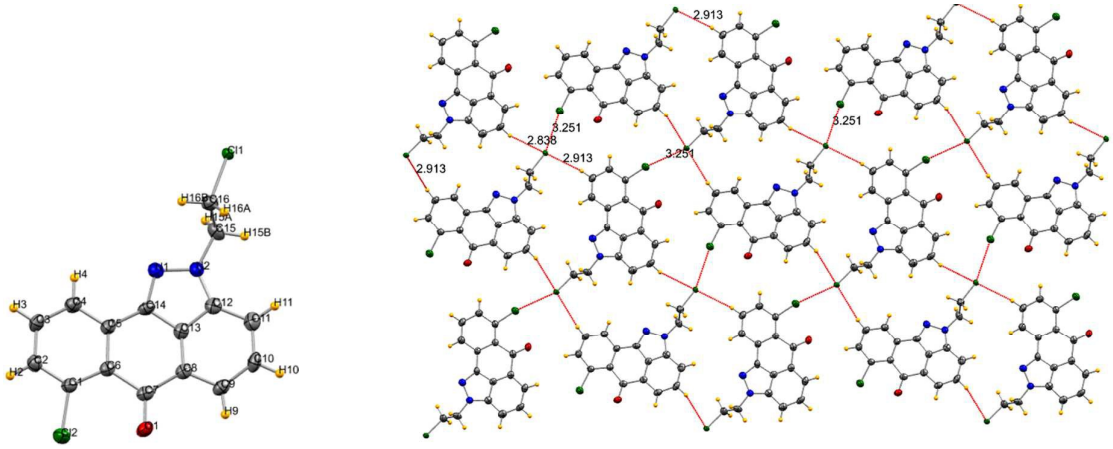

Fig. 1 ORTEP diagram of **R2** and crystal packing showing the three short interactions (two C-H...Cl and one Cl...Cl).

Table 1 Crystallographic parameters of **R2**

Compound	**R2**
Formula	$C_{16}H_{10}Cl_2N_2O$
Formula weight	317.16
Crystal system	Monoclinic
Space group	$P2_1/n$
a (Å)	6.7039(5)
b (Å)	14.5890(10)
c (Å)	13.9378(9)
α (°)	90
β (°)	96.283(6)
γ (°)	90
Volume (Å^3)	1354.97(16)
Z	4
Temperature (K)	100.08(2)
Density (g cm^{-3})	1.555
μ (mm^{-1})	0.478
F (000)	648
$h_{min, max}$	-8, 8
$k_{min, max}$	-18, 18

View Article Online
DOI: 10.1039/C8NJ00852C

$l_{min, max}$	-17, 18
No. of measured reflections	18436
No. of unique reflections	3099
No. of reflections used	2314
$R_{\_all}$, $R_{\_obs}$	0.1271,0.0964
wR_{2_all}, wR_{2_obs}	0.2391, 0.2226
$\Delta\rho_{min, max}$ (e Å^{-3})	–0.506, 0.677
GOOF	1.111
CCDC No.	1560310

2.3. Optimization of JNK inhibitors through computational studies

The crystal structure of the protein JNK3 with the inhibitor SP600125, 1PMV (JNK3), along with two other structures 2NO3 (JNK1) and 3E7O (JNK2) have been selected for the *in silico* studies from the Protein Data Bank. The crystal structure 1PMV (JNK3) indicates that the hydrophobic inhibitor (SP600125) interacts with the protein *via* hydrogen bonds with the carbonyl oxygen of Glu147 and the main chain nitrogen of Met149, in addition to several hydrophobic contacts with Ile70, Ala91, Met146, Leu148, Asp150, Asn152, Val196 and Leu206 respectively[39] (Fig. S2A, ESI†). It is noteworthy that on superposition of the active site of AMP-PCP bound JNK3 with that of the inhibitor-bound JNK3 (1PMV), it is found that SP600125 molecule binds to the hydrophobic adenine binding site *via* conserved hydrogen bonds with the backbone (Met149[N] and Glu147[O]). Additionally, computational alanine-scanning results show that Ile70, Leu206, Val196 are important for SP600125 recognition (Fig. S2B, ESI†).

Although the crystal structure of JNK3-SP600125 complex (1PMV) is already available,[39] docking calculations with the incorporation of the inhibitor at the active site were made to

View Article Online
DOI: 10.1039/C8NJ00852C

determine the least binding energy configuration (-8.05 Kcal mol^{-1}).[22,23] Similar calculations were performed with the other JNK's as well. It is observed that the binding of the inhibitors exhibit similar trends for all three JNKs, with subtle variations. The studies were extended to examine the propensity of binding with **R1**, **R2** and **R3** to evaluate the role of chlorine atoms in the binding pocket. It is noteworthy that, as the number of chlorine atoms increases, a decrease in binding energy is observed, suggesting favourable binding characteristics. The binding energies of **R1** and SP600125 are comparable in JNK2 and JNK3 (Table 2),[23] whereas **R2** and **R3**, have lower binding energies compared to **R1** and SP600125. An analysis of the protein-ligand interactions on the docked structures indicates that **R2** and **R3** exhibit several halogen contacts within the distance of 3.5Å (Table 2). In addition, conserved hydrogen bonds are seen between the ligands and the active site of the corresponding protein. However, it is of interest to note that in case of **R2**, the hydrogen bonding interaction is disrupted when binding to JNK1. It may be concluded that the presence of halogen interactions along with hydrogen bonds suggest better binding characteristics of **R2** and **R3** compared to that of **R1**(Table 2) (Fig. S3a–S3c, ESI†). A comprehensive analysis of the binding characteristics (halogen bonding) will be obtained from the crystal structures of all JNK's with R1, R2 and R3 respectively and crystallization experiments are currently being pursued.

Table 2 Analysis of halogen interactions among the JNKs (1PMV: JNK3, 3E7O: JNK2, 2NO3: JNK1) and the ligand molecules. The halogen contacts were determined using PLIP server.

View Article Online
DOI: 10.1039/C8NJ00852C

Protein, ligand complex	Binding Energy (kcal/mol)	Hydrogen bond with active site residue	Possible predictable halogen bonds between the protein atom and ligand atom	All halogen contacts*
1PMV, **R1**	-8.08	with Met149	Cl...O(Gly76)	Cl...CG2(Val78)
1PMV, **R2**	-8.75	with Met149	Cl_X....O(Met149)	Cl....NZ(LYS93) Cl....HZ2(LYS93) Cl....HZ3(LYS93)
1PMV, **R3**	-8.44	with Met149	Not detected	Cl....N(GLY73) Cl....CG2(VAL78) Cl_Y....O(MET149)
2NO3, **R1**	-6.69	with Asn 114	Not detected	Cl....CD1(ILE86) Cl....HN(MET111) Cl....CG2(VAL158)
2NO3, **R2**	-6.75	Not detected	Cl...O(Gly38)	Cl_X....O(MET111)
2NO3, **R3**	-6.73	with Met111	Not detected	Cl....HN(GLY35) Cl....CG2(VAL40) Cl_Y..HN(MET111)
3E7O, **R1**	-7.95	with Met111	Not detected	Cl....NZ(LYS55) Cl....HZ2(LYS55) Cl....HZ3(LYS55) Cl....O(LEU168)
3E7O, **R2**	-8.64	with Met111	Cl_X....O(Met111)	Cl....NZ(LYS55) Cl....HZ2(LYS55) Cl....HZ3(LYS55) Cl....O(LEU168) Cl_X....N(ALA113)
3E7O, **R3**	-8.20	with Met111	Cl_Y....O(Gly38)	Cl....O(SER34) Cl....CG2(VAL40) Cl_Y..CB(MET108) Cl....O(GLU109)

* The halogen contacts (<3.5Å) are only considered.

2.4. Molecular dynamics simulations

View Article Online
DOI: 10.1039/C8NJ00852C

Molecular dynamics simulations were carried out of ligand bound protein complexes (**R1**, **R2**, **R3** and PDB id:1PMV) to examine the stability of the protein molecules in the presence of ligands. The ligand bound simulations showed overall stabilization of the protein molecule compared to that of the *apo* protein as is evidenced by the lowering of RMSD (Fig. 2A). All three ligands form an average of one hydrogen bond throughout the trajectory. The distances between interacting atoms involved in halogen contacts in **R1**, **R2** and **R3** were computed from the co-simulations trajectory. It is noteworthy that the contact distances extracted from

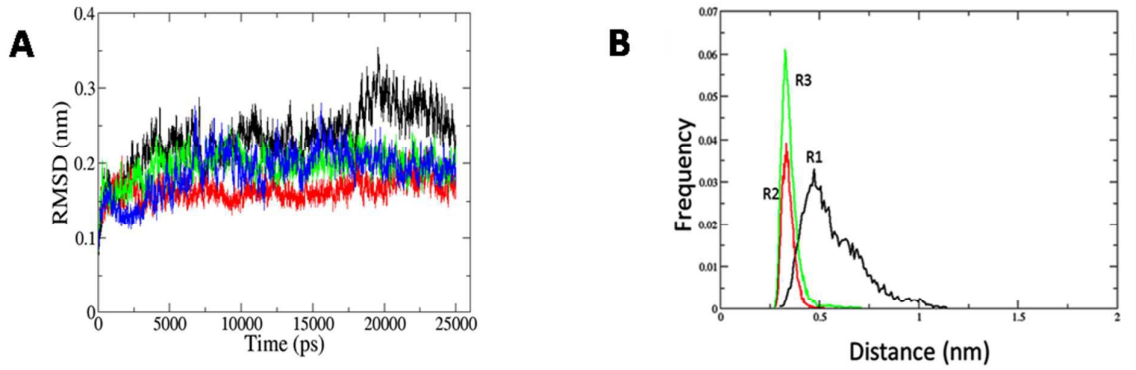

Fig. 2 (**A**) RMSD plot (Black: *apo* form; Red: **R1**; Green: **R2**; Blue: **R3**) extracted from the molecular dynamics simulations of *apo* and *holo* (**R1**, **R2**, **R3**) forms of JNK3 reveals that the protein is stable in the presence of all three ligands at the active site. (**B**) The distribution of the length of the halogen interactions are shown for all three holo simulations (Black: **R1**; Red: **R2**; Green: **R3**).

R2 and **R3** simulations have a narrow distribution with peaks around 3.5Å, (which imply stable interactions at an optimal distance for halogen contact), whereas **R1** has a wider distribution with a peak at 5Å, suggesting weaker propensity for halogen interactions (Fig. 2B).

2.5. Biological Evaluation

2.5.1. *In vitro* cytotoxic studies towards cell viability

The primary screen was performed to examine the cytotoxic effect of analogues of 1,9-pyrazoloanthrone (SP600125, **R1**, **R2**, and **R3**) on macrophages. Careful titration with

View Article Online
DOI: 10.1039/C8NJ00852C

analogues displayed significant cytotoxicity for inhibitor only above 30μM concentration (Fig. 3).

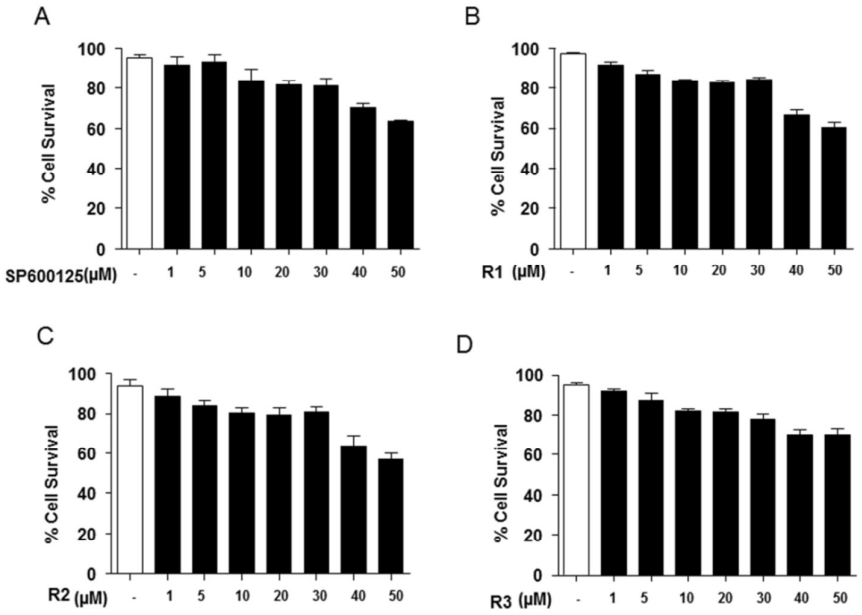

Fig. 3 MTT assay was performed to assess viability of mouse peritoneal macrophages upon treatment with varied concentration of **(A)** SP600125, **(B)** R1, **(C)** R2, and **(D)** R3 for 12 hours.

Based on these observation, less than 30μM concentration was used to assess inhibitory potential of analogues for JNK activity. Since, transcription factor, c-Jun is the well-characterized direct phosphorylation substrate of JNK, the activatory-phosphorylation status of c-Jun was taken as read out of JNKs activity. Furthermore, other members of MAPKs family such as ERK1/2 and p38 were analysed to assess the specificity of indicated inhibitors (SP600125, **R1**, **R2**, and **R3**). In agreement with the existing literature, primary macrophages treated with LPS were found to display elevated levels of phosphorylated-ERK1/2, p38 and c-Jun while upon treatment with inhibitors, macrophages showed a significant decrease in LPS-induced phosphorylation of c-Jun in accordance with indicated concentration of inhibitors. Importantly, **R3** showed reduced phosphorylation of c-Jun at 5μM concentration

View Article Online
DOI: 10.1039/C8NJ00852C

without affecting the phosphorylation status of other MAPKs, while **R1** and **R2** showed off target effects on pERK1/2 and pp38 (Fig. 4).

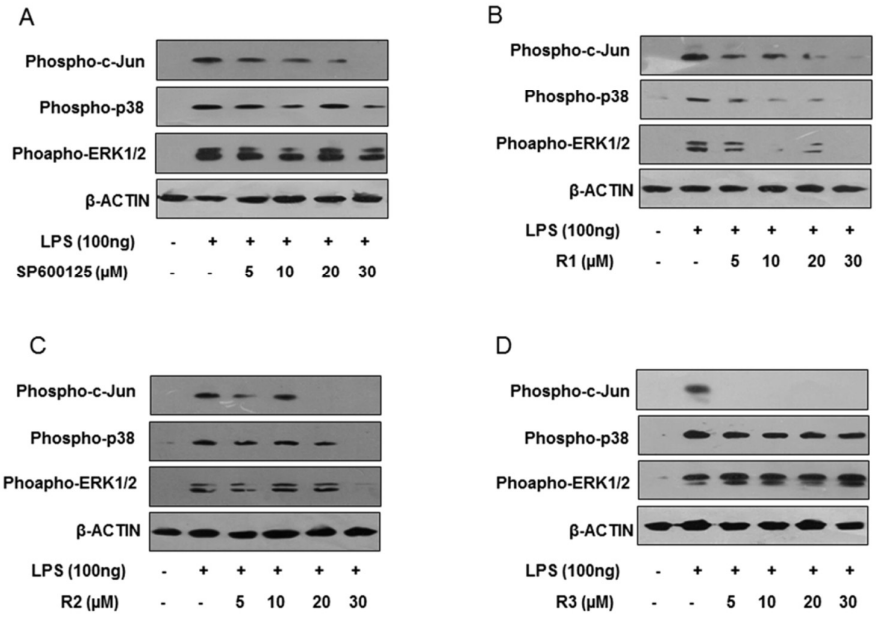

Fig. 4 R3 specifically inhibits c-Jun activity**.** Mouse peritoneal macrophages were treated with **(A)** SP600125, **(B)** R1, **(C)** R2, and **(D)** R3 for 1h prior to 12h treatment with LPS and phosphorylation status of c-Jun, p38 and ERK1/2 was analysed by immunoblotting.

Moreover, inhibitor treatment significantly diminished LPS induced promoter activity of AP1 which is mediated by JNK signalling as depicted in (Fig. 5**)**. Altogether, these results establish **R3** as a potent inhibitor of JNK activity at a dose as low as 1μM without off-target effects on ERK1/2 and p38 (Fig. 6). Thus, the potential of **R3** as a better inhibitor with superior selectivity is not just in comparison with the other inhibitors **R1** and **R2** but remarkably with that of the commercially utilized SP600125 is unequivocally established.

2.5.2. *Ex vivo* expression of LPS induced chemokines

At this stage, it is clear that **R3** is the best possible choice available as a new superior inhibitor of JNK and hence its contribution in modulating LPS-triggered responses is carried

View Article Online
DOI: 10.1039/C8NJ00852C

out. Interestingly, the host immune response to LPS is characterized by elevated chemokines expression *in vitro* as well *in vivo*[40] and some of the chemokines are JNK dependent.

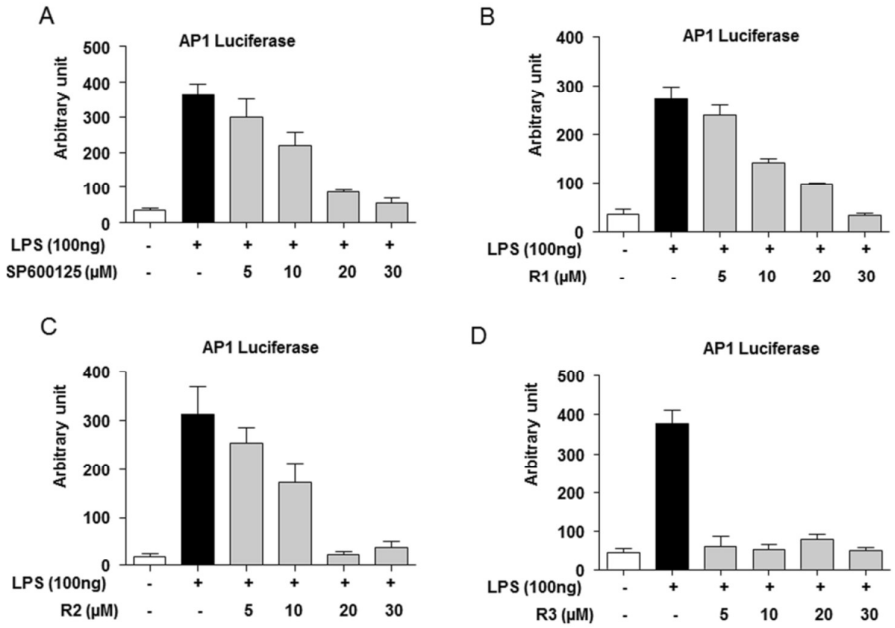

Fig. 5 Luciferase assay was performed on AP1 luciferase and β-galactosidase co-transfected murine RAW264.7 macrophages and treatment with **(A)** SP600125, **(B)** R1, **(C)** R2, and **(D)** R3 for 1h was given prior to LPS treatment for 12h.

It was observed that macrophages treated with 1μM **R3** exhibited diminished expression of LPS-induced chemokines (Fig. 7). This data thus strongly suggests **R3** as a potential regulator of LPS-triggered host immune response.

View Article Online
DOI: 10.1039/C8NJ00852C

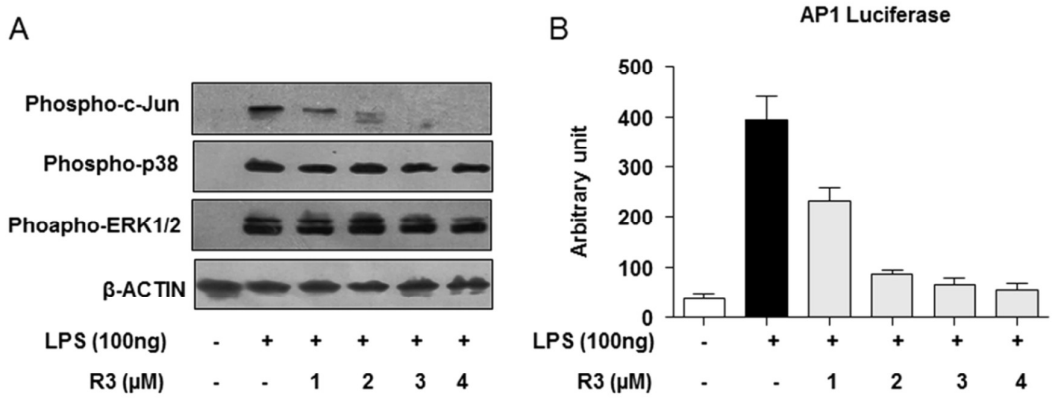

Fig. 6 Activity of c-Jun is specifically inhibited by R3 at lower concentrations. **(A)** Mouse peritoneal macrophages were treated with **R3** inhibitor for 1h prior to LPS treatment for 12h and phosphorylation status of c-Jun, p38, and ERK1/2 was analysed by immunoblotting. **(B)** Murine RAW264.7 macrophages were transiently co-transfected with AP1 luciferase and β-galactosidase luciferase followed by indicated inhibitors treatment for 1h prior to LPS treatment for 12h and luciferase assay was performed.

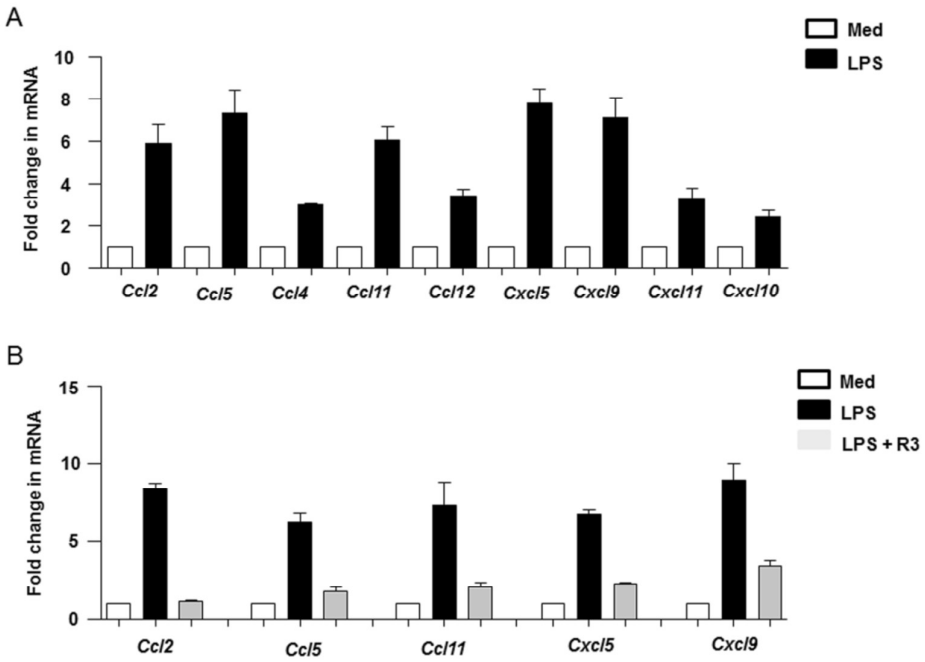

View Article Online
DOI: 10.1039/C8NJ00852C

Fig. 7 R3 attenuates expression of LPS-induced chemokines in macrophages. **(A)** Mouse peritoneal macrophages were treated with LPS for 12h and expression of indicated chemokines were analysed by quantitative real time RT-PCR. **(B)** Mouse peritoneal macrophages were treated with **R3** inhibitor 1h prior to LPS treatment and incubated for 12h and expression of indicated chemokines were analysed by quantitative real time RT-PCR.

3. Conclusions

In summary, we have designed and synthesized three halogenated derivatives of 1,9-pyrazoloanthrone. The involvement of halogen bonding provides highly directional interactions in the binding pocket and hence demonstrate improved inhibitory activity. Among the three halogenated derivatives of 1,9-pyrazoloanthrone, **R3** exhibits the most specific inhibition of JNKs activity at significantly lower concentrations (1μM) compared to **R1**, **R2**, and SP600125 with no off-target effects on other kinases such as p38 and ERK1/2. Further, **R3**, being a potent and specific inhibitor of JNKs, regulates LPS-triggered expressions of chemokines in macrophages. **R3** appears as the best designed inhibitor and hence may facilitate the development of novel therapeutics to treat JNKs-associated disorders. Therefore, current study proposes **R3** as a better alternative for SP600125 to inhibit JNKs activity and may act as a promising tool to comprehend the physiological role of JNKs for therapeutic benefits.

4. Experimental section

4.1. Chemical synthetic procedure

4.1.1. General information

All chemicals (Analytical grade) were purchased from Sigma-Aldrich and were used without additional purification. Solvents were purified according to standard methods. ^{1}H and ^{13}C-NMR spectra (400 and 100 MHz) were recorded on Bruker avance III-400 MHz NMR

View Article Online
DOI: 10.1039/C8NJ00852C

spectrometer at 25°C, using tetramethylsilane (TMS) as the internal standard. Chemical shifts were reported in ppm. HR-MS was obtained using a micromass-QTOF spectrometer using electrospray ionization (ESI).

4.1.2. Synthesis of 2-(2-chloroethyl)dibenzo[*cd,g*]indazol-6(2*H*)-one (R1).

This compound is prepared according to the modified procedures.[41–43] In 50 mL round bottom flask, 1,9-pyrazoloanthrone (220 mg, 1mmol) was dissolved in dimethylformamide (DMF) (2 mL) and K_2CO_3 (138 mg, 1 mmol) was added and stirred for 30 min. To this reaction mixture, 1-bromo-2-chloroethane (142 mg, 1 mmol) was added slowly and stirred overnight at 100°C. The formation of **R1** was monitored by TLC. After completion of the reaction, DMF was removed using high vacuum rotary evaporator. The reaction mixture was dissolved in ethyl acetate and extracted with water. The combined organic layers were washed with brine, dried over anhydrous Na_2SO_4 and concentrated *in vacuo*. Further the crude mixture was purified through silica gel column chromatography and recrystallized in dichloromethane and methanol mixture gives light yellow solid. Yield: 76 %. ^{1}H NMR (400 MHz, $CDCl_3$): δ 8.43 (dd, J = 8.0 Hz, 0.8 Hz, 1H), 8.18 (dd, J = 7.6 Hz, 0.8 Hz, 1H), 8.03 (d, J = 6.8 Hz, 1H), 7.74-7.63 (m, 3H), 7.54 (dt, J = 8.0 Hz, 1.2 Hz, 1H), 4.81 (t, J = 6.4 Hz, 2H), 4.07 (t, J = 6.0 Hz, 2H). ^{13}C NMR (100 MHz, $CDCl_3$): δ 183.5, 139.8, 133.3, 133.2, 131.4, 129.1, 128.6, 128.5, 126.3, 123.4, 122.7, 120.8, 114.8, 51.3, 42.9. HRMS: *m/z* calcd. for $C_{16}H_{11}ClN_2O$:calcd. 305.0458 $[M+Na]^+$; found 305.0455

4.1.3. Synthesis of 7-chloro-2-(2-chloroethyl)dibenzo[*cd,g*]indazol-6(2H)-one (R2).

This compound was synthesized similar to **R1**, but 5-chloro-1,9-pyrazoloanthrone was used. The crude mixture was purified through silica gel column chromatography and recrystallized in chloroform and methanol mixture gives brownish solid. Yield: 68 %. ^{1}H NMR (400 MHz, $CDCl_3$): δ 8.18 (dd, J =3.2 Hz, 2.8 Hz, 1H), 8.01 (d, J =6.8 Hz, 1H), 7.73 (d, J =8.0 Hz, 1H), 7.69- 7.65 (m, 1H), 7.56- 7.55 (m, 1H), 4.82 (t, J =6.4 Hz, 2H), 4.07 (t, J =6.0 Hz, 2H). ^{13}C

View Article Online
DOI: 10.1039/C8NJ00852C

NMR (100 MHz, $CDCl_3$): δ 182.4, 139.7, 139.1, 137.2, 134.3, 132.9, 132.8, 129.1, 128.9, 126.9, 122.6, 121.8, 121.1, 114.6, 51.4, 42.9. HR-MS: *m/z* calcd. for $C_{16}H_{10}Cl_2N_2O$; calcd. 317.0248 $[M+H]^+$; found 317.0248

4.1.4. Synthesis of 5-chloro-2-(2-chloroethyl) dibenzo[*cd,g*]indazol-6(2H)-one (R3).

This compound was synthesized as similar to **R1**, but 4-chloro-1,9-pyrazoloanthrone was used. The crude mixture was purified through silica gel column chromatography and recrystallized in dichloromethane and methanol mixture gives light yellow solid. Yield: 62 %. ^{1}H NMR (400 MHz, $CDCl_3$): δ 8.44 (dd, *J* =8.0 Hz, 0.8 Hz, 1H), 8.15 (dd, *J* =8.0 Hz, 0.9 Hz, 1H), 7.70 (td, *J* =8.0 Hz, 1.6 Hz, 1H), 7.69-7.48 (m, 3H), 4.79 (t, *J* =6.0 Hz, 2H), 4.07 (t, *J* =6.0 Hz, 2H). ^{13}C NMR (100 MHz, $CDCl_3$): δ 181.5, 139.2, 138.5, 133.3, 133.2, 131.6, 130.6, 129.3, 129.0, 128.8, 124.1, 122.4, 121.8, 115.3, 109.1, 51.5, 43.0. HR-MS: *m/z* calcd. for $C_{16}H_{10}Cl_2N_2O$; calcd. 317.0248 $[M+H]^+$; found 317.0248

4.2. Single crystal X-ray diffraction

X-ray diffraction data on suitable single crystals were collected on an Oxford Xcalibur Mova E diffractometer equipped with an EOS CCD detector and a micro focus sealed tube using Mo Kα radiation (λ = 0.71073 Å) at 100K using an Oxford Cobra open stream non-liquid nitrogen cooling device. Data collection and reduction were performed using CrysAlisPro (version 1.171.36.32)[44] and OLEX2 (version 1.2)[45] was used to solve and refine the crystal structures. All non-hydrogen atoms were refined anisotropically and H-atoms were located geometrically and refined isotropically. The WinGX[46] package was used for final refinement, production of CIFs and crystallographic table and ORTEP-3[47] for structure visualization and making the molecular representations. Packing diagrams were generated by using MERCURY.[48]

View Article Online
DOI: 10.1039/C8NJ00852C

4.3. *In Silico* studies

4.3.1. Ligand preparation, docking and analyses

The three-dimensional (3D) structures of **R1**, **R2**, and **R3** were modelled and minimised using the PRODRG server[49] since only one crystal structure was available. AutoDock (version 4.2)[50] was used for the ligand-protein docking. The Lamarckian Genetic Algorithm was used with a population of 200 dockings. The docking output was analysed using PLIP,[50] Pymol and Ligplot.[51] Hydrogen bonds were determined using the in-built HBPLUS[52] module in Ligplot with hydrogen bonding parameters (D-A distance ≤3.35 Å, H...A ≤2.7 Å), while halogen interactions were calculated using the Protein Structure Analysis Package (PSAP)[53] with D-X distance ≤3.5 Å, where X is the halogen atom. Computational alanine scanning was also performed on ligand bound structures obtained from docking and ABS-scan server[54] was used for that purpose.

4.3.2. Molecular dynamics

Molecular dynamics (MD) simulations were performed on JNK3 (PDB-id: 1PMV) in *apo* form and with each of **R1**, **R2**, and **R3** bound to it. Water molecules and hetero atoms were removed from the PDBs, while the missing atoms and loops were modelled using SWISS-MODEL.[55] SwissParam[56] web-server was used to generate parameter files for the small molecules compatible with the CHARMM force field. MD simulation was run using the GROMACS 4.5.3 package[57] with CHARMM all atom force field[58] and SPC/E water model.[59] The protein was simulated in a dodecahedron box with a distance of 10Å between the box and the protein. Cl^- ions were added to neutralize unbalanced charges on the protein. Particle Mesh Ewald (PME) method[60] was used for treating the electrostatic interactions. The bond lengths were constrained using the LINCS algorithm.[61] The system was energy minimized using the conjugate gradient algorithm with convergence criteria of 1 kJ mol^{-1} nm^{-1} to

View Article Online
DOI: 10.1039/C8NJ00852C

eradicate all short contacts. Thereafter, the system was coupled to a temperature bath using the Nosé-Hoover thermostat.[62,63] The pressure of the system was isotropically (compressibility of 4.5×10^{-5} bar^{-1}) coupled to a barostat at 1 bar using the Parrinello-Rahman method.[64] The position restrained dynamics was run for 100ps during both temperature and pressure equilibration. Simulation was run with a time step of 2fs, while the atomic coordinates and velocities were saved for every 2ps. Production simulation was run for a period of 25ns.

4.4. Biological assays

4.4.1. Reagents and antibodies

General laboratory chemicals were obtained from Sigma-Aldrich, Merck, HiMedia and Promega. Tissue culture plasticware was purchased from Corning Inc. or Tarsons. LPS was purchased from Sigma (USA). Phospho-c-Jun, Phospho-ERK1/2, and Phospho-p38 antibodies were obtained from Cell Signaling Technology (USA).

4.4.2. Cells and mice

RAW 264.7 mouse macrophage cell line was obtained from the National Center for Cell Sciences, Pune, India and was cultured in Dulbecco's modified Eagle medium (DMEM) (Gibco-Life Technologies) supplemented with 10% heat-inactivated FBS (Gibco-Life Technologies), maintained at 37°C in 5% CO_2 incubator. Primary macrophages were obtained from peritoneal exudates of C57BL/6 WT and BALB/cJ mice. All strains of mice were purchased from The Jackson Laboratory and maintained in the Central Animal Facility (CAF), Indian Institute of Science (IISc).

4.4.3. MTT assay

10,000 cells were seeded to wells of 96 well microtiter plate. After 24 hours, when the monolayer formed, the supernatant was flicked off and 100 µl of indicated supernatants were

View Article Online
DOI: 10.1039/C8NJ00852C

added to the cell in microtiter plate and kept for incubation at 37°C in 5% CO_2 incubator for 12 hours. After 12 hours, supernatant was flicked off and 50 µl of MTT dye was added to wells. The plates were gently shaken and incubated for 4 hours at 37°C in 5% CO_2 incubator. The supernatant was removed, 50 µl of DMSO was added, and the plates were gently shaken to solubilize the formed formazan. The absorbance was measured using a microplate reader at a wavelength of 595nm and the percentage of cell survival was calculated.

4.4.4. Transfection studies and Luciferase assay

RAW 264.7 macrophages were transiently transfected with desired plasmids using low m.w. polyehtylenimine (PEI). Transfection efficiency was more than 70% in all the experiments as determined by counting the number of siGLO Lamin A/C positive cells in several microscopic fields using fluorescent microscope. In all cases, 48h post-transfection, the cells were treated as indicated and processed for analysis. Treated cells were lysed in Reporter Lysis Buffer (Promega) and assayed for luciferase activity using Luciferase Assay Reagent (Promega) as per the manufacturer's instructions. The results were normalized for transfection efficiency measured by galactosidase activity. *o*-nitrophenol β-D-galactopyranoside (HiMedia) was utilized as substrate for the galactosidase assay.

4.4.5. RNA isolation and quantitative real-time RT-PCR

Macrophages were treated as indicated and total RNA from macrophages was isolated by TRI reagent (Sigma-Aldrich). 1.5 µg of total RNA was converted into cDNA using a First Strand cDNA synthesis kit (Bioline). Quantitative real-time RT-PCR was performed using SYBR Green PCR mixture (KAPA Biosystems) for quantification of the target gene expression. All the experiments were repeated at least 3 times independently to ensure the reproducibility of the results. *Gapdh* was used as an internal control. The primers utilised for quantitative real-time RT-PCR amplification are listed (Table S1, ESI†).

View Article Online
DOI: 10.1039/C8NJ00852C

4.4.6. Immunoblotting

Treated cells were pelleted and lysed in RIPA buffer [50 mM Tris-HCl (pH 7.4), 1% NP-40, 0.25% sodium deoxycholate, 150 mM NaCl, 1 mM EDTA, 1 mM PMSF, 1 μg/ml each of aprotinin, leupeptin, pepstatin, 1 mM Na_3VO_4, 1 mM NaF] on ice for 30 min. Whole cell lysates were collected and an equal amount of protein from each cell lysate was subjected to SDS-PAGE and transferred onto PVDF membranes (Millipore) by semi-dry Western blotting method (Bio-Rad). Nonspecific binding was blocked with 5% non-fat dry milk powder in TBST [20 mM Tris-HCl (pH 7.4), 137 mM NaCl, and 0.1% Tween 20] for 60 min. The blots were incubated overnight at 4ºC with primary antibody diluted in TBST with 5% BSA. After washing with TBST, blots were incubated with anti-rabbit or anti-mouse IgG secondary antibodies conjugated to HRP for 2h. The immunoblots were developed with enhanced chemiluminescence detection system (PerkinElmer) as per manufacturer's instructions and β-ACTIN was used as loading control. For probing another protein in the same region of PVDF membrane, the blots were stripped in the stripping buffer [62.5 mM Tris-HCl (pH 6.8), 2% SDS and 0.7% β-mercaptoethanol] at 60^{o}C on a shaker and followed by the same procedure as mentioned above.

4.4.7. Statistical analysis

Levels of significance for comparison between samples were determined by the Student *t*-test distribution and one-way ANOVA. The data in the graphs are expressed as the mean ± SE for 6 values from 3 independent experiments and P values < 0.05 were defined as significant. GraphPad Prism 5.0 software (GraphPad Software) was used for all the statistical analysis.

†Electronic Supplementary Information (ESI)

NMR data, HR-MS, Computational alanine result, and Gene primers.

View Article Online
DOI: 10.1039/C8NJ00852C

Conflicts of interest

There are no conflicts to declare.

Acknowledgments

This work was supported by funds from the Department of Biotechnology (DBT), Department of Science and Technology (DST), Council for Scientific and Industrial Research (CSIR) and Indian Council of Medical Research (ICMR), Government of India and the Indo-French Center for Promotion of Advanced Research (CEFIPRA) (Reference number 4803-1). We sincerely thank Dr. Gianluca Aguiari, Universita degli studi di Ferrara, Italy for 7XAP1 luciferase construct and Mr. Bharat Bhatt from KNB lab for useful discussions. RG and VS thank CSIR for the Senior Research Fellowship. KNB and TNG thank DST for the J. C. Bose Fellowship.

Abbreviations

LPS	Lipopolysaccharide
ERK	Extracellular signal regulated kinase
ADME/T	Absoption, Distribution, Metabolism, Excretion, and Toxicity
NMR	Nuclear Magnetic Resonance
ORTEP	Oak Ridge Thermal Ellipsoid Plot
MTT	3-(4,5-Dimethylthiazol-2-yl)-2,5-Diphenyltetrazolium Bromide
RT-PCR	Reverse transcription polymerase chain reaction

References

1 B. L. Bennett, Y. Satoh and A. J. Lewis, *Curr. Opin. Pharmacol.*, 2003, **3**, 420–425.

2 M. A. Bogoyevitch, I. Boehm, A. Oakley, A. J. Ketterman and R. K. Barr, *Biochim. Biophys. Acta*, 2004, **1697**, 89–101.

View Article Online
DOI: 10.1039/C8NJ00852C

3 M. A. Bogoyevitch, K. R. Ngoei, T. T. Zhao, Y. Y. Yeap and D. C. Ng, *Biochim. Biophys. Acta*, 2010, **1804**, 463–475.

4 K. Bandow, J. Kusuyama, M. Shamoto, K. Kakimoto, T. Ohnishi and T. Matsuguchi, *FEBS Lett*., 2012, **586**, 1540–1546.

5 R. Medzhitov and T. Horng, *Nat. Rev. Immunol*., 2009, **9**, 692–703.

6 L. Bendall, *Histol. Histopathol*., 2005, **20**, 907–926.

7 V. L. Bryant and C. A. Slade, *Immunol. Cell Biol*., 2015, **93**, 364–371.

8 C. Gerard and B. J. Rollins, *Nat. Immunol*., 2001, **2**, 108–115.

9 H. M. Lo, T. H. Lai, C. H. Li and W. B. Wu**,** *Acta Pharmacol. Sin*., 2014, **35**, 339–350.

10 H. M. Lo, J. M. Shieh, C. L. Chen, C. J. Tsou and W. B. Wu**,** *Int. J. Mol. Sci*., 2013, **14**, 10090–10106.

11 N. P. Shanware, K. Bray, C. H. Eng, F. Wang, M. Follettie, J. Myers, V. R. Fantin and R. T. Abraham, *Nat. Commun*., 2014, **5**, 4900.

12 K. H. Kim, D. R. An, J. Song, J. Y. Yoon, H. S. Kim, H. J. Yoon, H. N. Im, J. Kim, D. J. Kim, S. J. Lee, K. H. Kim, H. M. Lee, H. J. Kim, E. K. Jo, J. Y. Lee and S. W. Suh, *Proc. Natl. Acad. Sci. U. S. A*., 2012, **109**, 7729–7734.

13 Y. Liu, E. G. Shepherd and L. D. Nelin, *Nat. Rev. Immunol*., 2007, **7**, 202–212.

14 S. Marudhupandiyan and K. Balamurugan, *Immunol. Res*., 2017, **65**, 609–621.

15 P. Koch, M. Gehringer and S. A. Laufer, *J. Med. Chem*., 2015, **58**, 72–95.

16 B. L. Bennett, D. T. Sasaki, B. W. Murray, E. C. O'Leary, S. T. Sakata, W. Xu, J. C. Leisten, A. Motiwala, S. Pierce, Y. Satoh, S. S. Bhagwat, A. M. Manning and D. W. Anderson, *Proc. Natl. Acad. Sci. U. S. A*., 2001, **98**, 13681–13686.

17 J. Bain, H. McLauchlan, M. Elliott and P. Cohen, *Biochem. J*., 2003, **371**, 199–204.

View Article Online
DOI: 10.1039/C8NJ00852C

18 J. Bain, L. Plater, M. Elliott, N. Shpiro, C. J. Hastie, H. McLauchlan, I. Klevernic, J. S. Arthur, D. R. Alessi and P. Cohen**,** *Biochem. J*., 2007, **408**, 297–315.

19 M. L. H. Chu, L. M. G. Chavas, K. T. Douglas, P. A. Eyers and L. Tabernero**,** *J. Biol. Chem*., 2008, **283**, 21495–21500.

20 K. Miyazawa, *J. Biochem*., 2011, **150**, 1–3.

21 S. Tanemura, H. Momose, N. Shimizu, D. Kitagawa, J. Seo, T. Yamasaki, K. Nakagawa, H. Kajiho, J. M. Penninger, T. Katada and H. Nishina, *J. Biochem*., 2009, **145**, 345–354.

22 K. D. Prasad, J. Trinath, A. Biswas, K. Sekar, K. N. Balaji and T. N. Guru Row, *Org. Biomol. Chem*., 2014, **12**, 4656–4662.

23 K. D. Prasad, J. Trinath, A. Biswas, K. Sekar, K. N. Balaji and T. N. Guru Row, *Sci. Rep*., 2014, **4**, 7214.

24 P. Metrangolo and G. Resnati, *Science*, 2008, **321**, 918–919.

25 A. R. Voth, F. A. Hays and P. S. Ho, *Proc. Natl. Acad. Sci. U. S. A*., 2007, **104**, 6188–6193.

26 G. Cavallo, P. Metrangolo, R. Milani, T. Pilati, A. Priimagi, G. Resnati and G. Terraneo, *Chem. Rev*., 2016, **116**, 2478–2601.

27 R. Wilcken, M. O. Zimmermann, A. Lange, A. C. Joerger and F. M. Boeckler, *J. Med. Chem.,* 2013*,* **56**, 1363–1388.

28 P. Politzer and J. S. Murray, *ChemPhysChem*, 2013, **14**, 278–294.

29 P. Politzer, J. S. Murray and T. Clark, *Phys. Chem. Chem. Phys*., 2013, **15**, 11178–11189.

30 V. R. Hathwar and T. N. G. Row, *J. Phys. Chem. A*., 2010, **114**, 13434–13441.

31 V. R. Hathwar and T. N. G. Row, *Cryst. Growth Des*., 2011, **11**, 1338–1346.

View Article Online
DOI: 10.1039/C8NJ00852C

32 Y. Lu, Y. Liu, Z. Xu, H. Li, H. Liu and W. Zhu, *Expert Opin. Drug.Discov*., 2012, **7**, 375–383.

33 Z. Xu, Z. Yang, Y. Liu, Y. Lu, K. Chen and W. Zhu, *J. Chem. Inf. Model*., 2014, **54**, 69–78.

34 J. Westbrook, Z. Feng, S. Jain, T. N. Bhat, N. Thanki, V. Ravichandran, G. L. Gilliland, W. F. Bluhm, H. Weissig, D. S. Greer, P. E. Bourne and H. M. Berman, *Nucleic Acids Res*., 2002, **30**, 245–248.

35 Y. Lu, T. Shi, Y. Wang, H. Yang, X. Yan, X. Luo, H. Jiang and W. Zhu, *J. Med. Chem*., 2009, **52**, 2854–2862.

36 P. Y. S. Lam, C. G. Clark, A. M. Smallwood and R. S. Alexander, The 238th ACS national meeting. ACS, Washington, DC, 2009, **58**.

37 P. Auffinger, F. A. Hays, E. Westhof and P. S. Ho, *Proc. Natl. Acad. Sci. U. S. A*., 2004, **101**, 16789–16794.

38 T. G. Row and R. Ganduri, *Acta Cryst*., 2017, A**70**, C1337.

39 G. Scapin, S. B. Patel, J. Lisnock, J. W. Becker and P. V. LoGrasso, *Chem. Biol*., 2003, **10**, 705–712.

40 K. M. Kopydlowski, C. A. Salkowski, M. J. Cody, N. van Rooijen, J. Major, T. A. Hamilton and S. N. Vogel, *J. Immunol*., 1999, **163**, 1537–1544.

41 H. D. H. Showalter, J. L. Johnson, J. M. Hoftiezer, W. R. Turner, L. M. Werbel, W. R. Leopold, J. L. Shillis, R. C. Jackson and E. F. Elslager, *J. Med. Chem*., 1987, **30**, 121–131.

42 W. Bradley and K. W. Geddes, *J. Chem. Soc*., 1952, **0**, 1630–1635.

43 M. Kim and D. F. Wiemer, *Tetrahedron Lett*., 2004, **45**, 4977–4980.

44 CrysAlisPro, ver. 1.171.36.32, Agilent Technologies UK Ltd: Yarnton, England, 2011.

View Article Online
DOI: 10.1039/C8NJ00852C

45 O. V. Dolomanov, A. J. Blake, N. R. Champness and M. Schröder, *J. Appl. Cryst*., 2003, **36**, 1283–1284.

46 L. J. Farrugia, *J. Appl. Cryst*., 1999, **32**, 837–838.

47 L. J. Farrugia, *J. Appl. Cryst*., 1997, **30**, 565.

48 C. F. Macrae, P. R. Edgington, P. McCabe, E. Pidcock, G. P. Shields, R. Taylor, M. Towler and J. Van de Streek, *J. Appl. Cryst*., 2006, **39**, 453–457.

49 A. W. Schuttelkopf and D. M. F. Van Aalten, *Acta Crystallogr. D*., 2004, **60**, 1355–1363.

50 G. M. Morris, R. Huey, W. Lindstrom, M. F. Sanner, R. K. Belew, D. S. Goodsell and A. J. Olson, *J. Comput. Chem*., 2009, **30**, 2785–2791.

51 S. Salentin, S. Schreiber, V. J. Haupt, M. F. Adasme and M. Schroeder, *Nucleic Acids Res*., 2015, **43**, 443–447.

52 I. K. McDonald and J. M. Thornton, *J. Mol. Biol.,* 1994, **238**, 777–793.

53 B. Balamurugan, M. N. A. Md. Roshan, B. S. Hameed, K. Sumathi, R. S. Kumar, A. Udayakumar, K. H. Venkatesh Babu, M. Kalaivani, G. Sowmiya, P. Sivasankari, S. Saravanan, C. V. Ranjani, K. Gopalakrishnan, K. N. Selvakumar, M. Jaikumar, T. Brindha, M. Daliah and K. Sekar, *J. Appl. Cryst.,* 2007, **40**, 773–777.

54 P. Anand, D. Nagarajan, S. Mukherjee and N. Chandra, *F1000Res*., 2014, doi: 10.12688/f1000research.5165.2.

55 K. Arnold, L. Bordoli, J. Kopp and T. Schwede, *Bioinformatics,* 2006, **22**, 195–201.

56 Y. Assenov, F. Ramirez, S. E. Schelhorn, T. Lengauer and M. Albrecht, *Bioinformatics*, 2008, **24**, 282–284.

57 B. Hess, C. Kutzner, D. V. Spoel and E. Lindahl, *J. Chem. Theory Comput*., 2008, **4,** 435–447.

View Article Online
DOI: 10.1039/C8NJ00852C

58 P. Bjelkmar, P. Larsson, M. A. Cuendet, B. Hess and E. Lindahl, *J. Chem. Theory Comput*., 2010, **6**, 459–466.

59 H. J. C. Berendsen, J. R. Grigera and T. P. Straatsma, *J. Phys. Chem*., 1987, **91**, 6269–6271.

60 T. Darden, D. York and L. Pedersen, *J. Chem. Phys*., 1993, **98**, 10089–10092.

61 B. Hess, H. Bekke, H. J. C. Berendsen and J. G. E. M. Fraaije, *J. Comput. Chem*., 1997, **18**, 1463–1472.

62 W. G. Hoover, *Phys. Rev. A*., 1985, **31**, 1695–1697.

63 S. Nosé, *J. Chem. Phys*., 1984, **81**, 511–519

64 M. Parrinello and A. Rahman, *J. Appl. Phys*., 1981, **52**, 7182–7190.

View Article Online
DOI: 10.1039/C8NJ00852C

Table of Contents and Graphical abstract

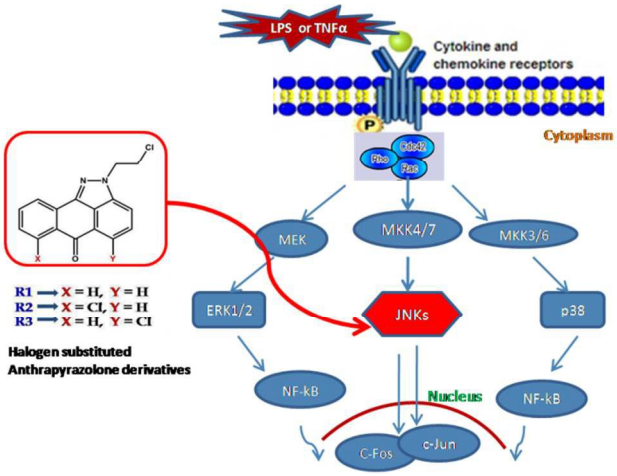

A specifically designed halogen substituted anthrapyrazolone derivatives for selective inhibition of JNKs activity at lower concentrations with minimal off-target effects on other kinases such as ERK1/2 and p38.